ELSEVIER

J. Non-Newtonian Fluid Mech. 128 (2005) 29–41

Journal of Non-Newtonian Fluid Mechanics

www.elsevier.com/locate/jnnfm

The melt processing of monodisperse and polydisperse polystyrene melts within a slit entry and exit flow

M.W. Collis, M.R. Mackley *

Department of Chemical Engineering, University of Cambridge, Pembroke Street, Cambridge CB2 3RA, UK

Received 21 October 2004; received in revised form 7 February 2005; accepted 12 February 2005

Abstract

This paper presents experimental results and numerical simulations for mono, blended and polydisperse polstryrenes of different molecular weights flowing within a slit geometry. Flow experiments were carried out on small (less than 10 g) quantities of polymer using a multi-pass rheometer and flow-induced birefringence images were obtained for well-defined flow boundary conditions. Experimental flow birefringence observations illustrate the similarities and differences in the flow behaviour between monodisperse and polydisperse polystyrene. For the case of monodisperse polystyrene a transition from "near-Newtonian" stress patterns for low molecular weight polystyrenes, to a highly unstable flow at high molecular weight was observed. Both blending and polydispersity enabled stable flows to be achieved at high flowrates.

Experimental flow birefringence results and some pressure difference predictions were compared with numerical predictions. Two different computational approaches were followed, one using a viscoelastic integral K-BKZ/Wagner model within the finite element method solver Polyflow, and the other using the tube theory-based Pom-Pom constitutive equation and Lagrangian-Eulerian code flowSolve. Both numerical methods were able to capture certain experimental observations reasonably well in the stable flow regime, but were not able to predict the onset of the experimentally observed flow instabilities.

Keywords: Flow birefringence; Multi-pass rheometer; Polymer melts; Polystyrene; Pom-Pom model; Wagner model

1. Introduction

In order to improve the understanding of the processing behaviour of polymer melts, there have been numerous papers comparing experimental measurements of physical properties such as pressure drop, flow-induced birefringence or velocity fields with numerical simulations of equivalent flow conditions (see for example [1–3]). In some cases constitutive equations have been tested in flow situations that are well defined, such as the flow into a capillary or slit and in other cases more complex geometries such as screw extruders have been modelled. In most "processing" flows, it has only been possible to examine commercially available samples because the supply of monodisperse polymer is very limited, however in this paper it was possible to rank the flow behaviour of both monodisperse polymer against a commercial polydisperse variant because the apparatus was configured to handle small quantities of material. Work described in this paper uses a multi-pass rheometer, [5,6] and this reciprocating piston rheometer can be configured to operate with quantities as small as 10 g. Each of the polymers were studied experimentally under well-defined flow conditions through a sudden narrow constriction, a geometry which contains areas of combined shear and extensional flow. The flow has analogies with more complex industrial processing situations and is a commonly referred to as a benchmark flow [4]. The ability of the MPR apparatus to measure pressure differences and to capture flow-induced birefringence images of polymer melt flows under controlled flow conditions has been demonstrated previously [3,7], however its application in ranking processibility for monodisperse polymers against polydisperse polymers is new. Within the context of this paper, polymer processibility is concerned with the way a par-

* Corresponding author.
E-mail address: mrm1@cheng.cam.ac.uk (M.R. Mackley).

0377-0257/$ – see front matter © 2005 Elsevier B.V. All rights reserved.
doi:10.1016/j.jnnfm.2005.02.010

ticular polymer flows in a steady flow regime within the flow geometry and also how the polymer may develop an unstable flow. Invariably polymer processing without flow instabilities is crucial to any successful commercial extrusion process.

The acquisition of experimental data for both mono and polydisperse polymers also enables comparison to made with currently available simulation and assists in the depth of understanding relating to processing. The ability to simulate the viscoelastic flow of polymer melts has improved significantly in recent years, as a result of more powerful computers, improved numerical methods for flow calculations [8], and the development of new constitutive models – such as the Pom-Pom model [9] – derived from molecular behaviour as alternatives to established models such as the K-BKZ [10] or generalized Maxwell model. In this paper, the experimental data is compared with two numerical schemes and this enables a comparison to made between current numerical predictions and experimental reality for both mono and polydisperse materials in a flow geometry that captures most elements of a "processing flow".

2. Experimental

2.1. Materials

The polymers used were all polystyrenes, and since they share a common chemical structure the differences between them could be linked to their differing molecular weight distributions. They were supplied by two sources – Dow Chemicals and the University of Durham. Five monodisperse polystyrenes with a range of molecular weights of approximately an order of magnitude were used. Bimodal polydispersity was introduced by blending together a pair of these in two proportions, and in addition experiments were performed using a commercial-style broadly polydisperse material. The properties of these polymers are summarised in Table 1.

2.2. Characterisation

Rheological characterisation of the polystyrenes was performed using dynamic strain and step strain experiments on a Rheometrics ARES rotational rheometer. A small fixed frequency strain sweep was used to determine the upper limit of the linear viscoelastic region to ensure that the characterisation was made within this region. The results of small amplitude frequency sweep tests were used with a non-linear regression curve fitting procedure in the rheometer's software to determine a linear relaxation spectrum for each polymer. It has been found that a spectrum with at least five relaxation times is needed to fit most data [11]. Increasing the number gives a small increase in precision but increases the complexity of the number of adjustable parameters used – here the use of eight relaxation times has been chosen. The Wagner non-linear damping factors were determined from a series of step strain experiments in which the sample was subjected to an instantaneous deformation at different magnitudes of strain, with the decaying relaxation modulus measured. As a check, the stress and apparent viscosity in steady shear over an increasing range of flow rates were shown to be consistent with the earlier results. A detailed description of the characterisation procedure that was used can be found in [12].

Table 1
Properties of the polystyrenes studied

Designation	Type	M_w (g/mol)	Polydispersity
Durham 66k PS	Monodisperse	67900	1.03
Dow PS1569	Monodisperse	204000	1.09
Durham 250k PS	Monodisperse	257800	1.03
Durham 485k PS	Monodisperse	500500	1.02
Dow PS1571	Monodisperse	510000	1.15
Durham 80% 485k/20% 66k PS	Blend	486400	1.20
Durham 90% 485k/10% 66k PS	Blend	494100	1.10
Dow PS680E	Polydisperse	219000	2.43

2.3. Processing experiments

The multi-pass rheometer (MPR4) that was used for the processing experiments was a dual piston capillary-type rheometer, which had been designed for small quantities of sample material and could make useful measurements with as little as 10 g of polymer. It consists of two hydraulically driven pistons mounted above and below a central test section, which can be controlled to move either independently or together in several different modes of operation. The top and bottom barrels contain pressure transducers and thermocouples to monitor the state of the system, and all three sections contain heating jackets through which silicone oil can be circulated for temperature control, up to 200 °C. A PC running custom software written in LabVIEW was used for controlling experimental procedure and for data acquisition and analysis. The layout of the MPR is shown in Fig. 1.

When the MPR system was loaded and sealed, the pistons could be used to set the mean pressure and to carry out a series of experiments at a range of shear rates and over a long period of time with the same small sample. There was no noticeable degradation of the samples over time, as a consequence of the enclosed nature of the system. The results presented here are from a single pass steady shear operation – the steady shear was generated by movement of the two pistons in unison at a constant velocity. In general, the pressure difference developed quickly across the test section, and for the rest of the stroke this pressure was seen to be constant. The symmetry of the geometry results in the same flow being generated in both directions, and the cycle can be repeated, hence multi-pass flow with inherent repetition within each experiment. In this paper, a range of piston speeds between 0.01 and 2.0 mm/s were used and in all cases a holding

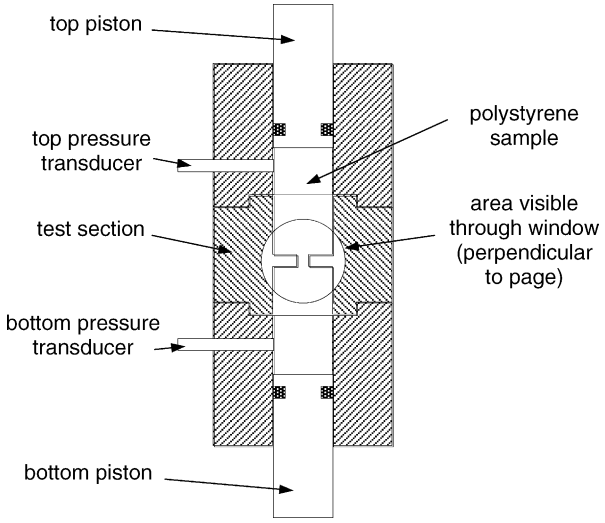

Fig. 1. Outline of MPR.

time of at least 1 min was applied between successive passes in order for the material to equilibrate between each pass.

The test section used was a slit flowcell, which enabled simultaneous rheological and optical measurements to be made. This resembles a cube with holes in all six faces, surrounded by heating channels and insulation. The polymer melt flows vertically, while the other faces accept a pair of slit die inserts in one direction, and a pair of stress-free windows in the other. The die inserts formed a contraction and expansion flow through a narrow slit, with the cross-section as shown in Fig. 2 and a depth of 10 mm. Within the slit the aspect ratio of the slit is 10 mm/0.9 mm and this gives a reasonable approximation to two-dimensional. Upstream and downstream of the slit the aspect ratio is 10 mm/10 mm.

Rheo-optical data was obtained using the flow-induced birefringence technique [13] to observe the stresses within the melt. Monochromatic polarised light with a wavelength of 514 nm was passed through the flowcell, then through an orthogonal analyser, and captured using a digital video camera. The variation in refractive indices within the test section retards one component of the electric vector in the light, and a pattern of bright and dark fringes can be seen. These fringes represent contours of equal retardation, and can be considered to correspond to contours of equal principal stress difference. Quarter wave plates were used in the optical train to eliminate the isoclinic extinction bands and leave only the stress-related isochromatics; in some cases image clarity was improved by their omission, so the isoclinics are visible but can be disregarded for comparative purposes. In this study, a two-dimensional retardation analysis was assumed with a stress optical coefficient of $-4.5 \times 10^{-9}\,\mathrm{Pa}^{-1}$ (see Section 4.5).

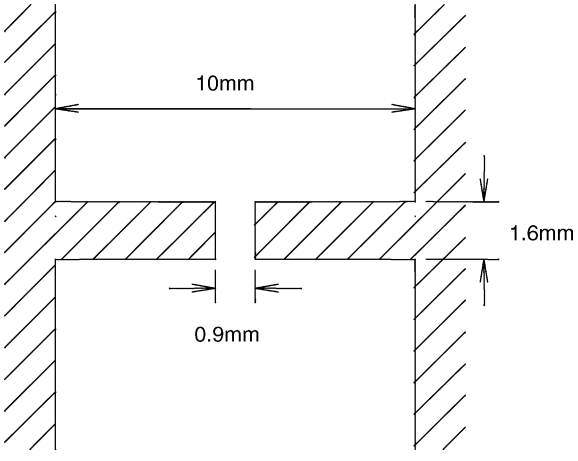

Fig. 2. MPR slit flowcell geometry.

3. Numerical simulation

When attempting to match numerical predictions to experimental data, there are a large number of potential parameters to take into account for the simulation, as well as the requirement that the flow rate, temperature and pressure conditions accurately reflect the experimental values. In the case of the multipass rheometer, the external geometrical and flowrate boundary conditions are specified with high precision. One aspect of choice, however, is the constitutive equation, and its associated set of parameters. Another is the software code used, with implied algorithm and implementation and chosen convergence criteria and grid layout. Finally, when comparisons are made between birefringence images and calculated stress fields the stress–optical relation connecting the two must be considered.

3.1. Constitutive models

Two different constitutive models have been applied to the polystyrenes representing contrasting approaches to the formulation of such a model. Common to both is the generalised Maxwell model for linear viscoelasticity (see for example [14]). The main differences are in the models' treatment of non-linear viscoelastic behaviour, which is important in any deformation that is neither very small nor very slow, including most polymer processing. One approach to account for non-linear viscoelasticity is by devising empirical relationships and relating these to experimental data; many examples of this type can be found in [15]. An alternative approach is to derive a physical model for the behaviour of long molecules and make simplifying assumptions to obtain a useable equation set, such as that taken by Doi and Edwards [16].

As a representative of the former approach, we have used the constitutive equation proposed by Wagner [17] and based on the K-BKZ equation [10] given in equation set (1) – this is subsequently referred to simply as the Wagner model. Irreversibility is a factor in complex processing geometries because the physical loss of entanglements occurs by both

thermal relaxation and strain-induced mechanisms, whereas entanglements reform only thermally (by Brownian motion). This is accounted for by using a minimum value of the damping function [18].

$$\begin{aligned}\boldsymbol{\sigma}(t) &= -\int_{-\infty}^{t} m(t-t')\min\{h(I_1, I_2)\}\boldsymbol{B}(t, t')\,\mathrm{d}t' \\ m(t-t') &= \sum_i \frac{g_i}{\lambda_i}\exp\left(\frac{-(t-t')}{\lambda_i}\right) \\ h(I_1, I_2) &= \exp\left(-k\sqrt{\beta I_1 + (1-\beta)I_2 - 3}\right)\end{aligned} \tag{1}$$

This contains a time-dependent memory function $m(t-t')$ and strain-dependent exponential damping function $h(I_1, I_2)$ with two non-linear parameters, the more important being the damping factor k. $\boldsymbol{B}(t, t')$ is the Finger strain tensor which describes deformation between past and present times t' and t. The memory function is expressed in terms of the linear relaxation spectrum g_i, λ_i and the damping function is in terms of the scalar invariants I_1 and I_2 of the Finger strain tensor.

For a molecular model we have used the Pom-Pom model of McLeish and Larson [9] which is based on tube theory for a branched molecular geometry having two q-armed stars connected by a backbone segment, with different characteristic relaxation times for the stretch (τ_s) and orientation (τ_b) of the backbone. For describing real polymers which do not conform to the theoretical geometry, the model has been extended to a multi-mode form [19] which represents the polymer with a spectrum of relaxation times that can be related to the proximity of different molecular segments to a free chain end. The central equation for stress is given in terms of backbone stretch $\lambda(t)$ and orientation tensor $\boldsymbol{S}(t)$, with subsidiary equations for the evolution of both of these quantities with time. A subsequent refinement to the model is the consideration of drag-strain coupling between relaxed and stressed chain segments, which adds an exponential term to the stretch equation [20]. Equation set (2) shows the Pom-Pom model as used for the numerical simulations in this paper.

$$\begin{aligned}\boldsymbol{\sigma}(t) &= \sum_i \boldsymbol{\sigma}_i = 3\sum_i g_i\lambda_i^2(t)\boldsymbol{S}_i(t) \\ \frac{D\boldsymbol{A}_i(t)}{Dt} &= \boldsymbol{\kappa}\cdot\boldsymbol{A}_i + \boldsymbol{A}_i\cdot\boldsymbol{\kappa}^T - \frac{1}{\tau_{bi}}(\boldsymbol{A}_i - \boldsymbol{I}), \\ \boldsymbol{S}_i(t) &= \frac{\boldsymbol{A}_i(t)}{tr\boldsymbol{A}_i(t)} \\ \frac{D\lambda_i(t)}{Dt} &= \lambda_i(t)\boldsymbol{\kappa} : \boldsymbol{S}_i - \frac{1}{\tau_{si}}(\lambda_i(t)-1)\,\exp\{\nu_i^*(\lambda_i(t)-1)\}, \\ \lambda_i &\le q_i\end{aligned} \tag{2}$$

Numerical simulation of entry flows using the Pom-Pom constitutive equation has already been carried out by Clemur et al. [21,22] and Lee et al. [23].

3.2. Software for solving flow problems

Two computer software programs have been used to simulate the polystyrene melt. In addition to the implementation of alternative approaches to model rheological behaviour, they also use different numerical solution methods, which gives a useful comparison between the two predictions via different routes as well as with observed experimental behaviour. In both cases, all the simulations performed were constrained to be two-dimensional and isothermal. The justification for isothermal simulation was based on the experimental ability to detect temperature changes greater than 2 °C using the observation of laser refraction effects through the sample. Several different computers were used for the simulations, all of which were PCs with ×86 family processors.

The first simulation was Polyflow [24], a commercial Eulerian finite element method [8] solver used widely for the simulation of polymer processing flows. The Eulerian scheme is implemented by defining a fixed mesh of quadrilateral elements, within each of which the conservation of mass and momentum is applied, solving for kinematics and stress in turn, taking multiple iterative steps until a converged solution is obtained. Polyflow was used for predictions using the integral Wagner/K-BKZ model. For integral viscoelastic flow problems, a three-stage process is used; first, an approximate generalised Newtonian solution is obtained as a starting point; then viscoelasticity is gradually introduced using an evolution algorithm, using the solution of each of a series of calculations as a basis for the next; finally the fully viscoelastic solution is refined using the result of the evolution stage with a more stringent convergence criterion. A previous application of this method to an MPR flow problem can be found in [7].

FlowSolve is a Lagrangian flow solver with an academic background, developed at the University of Leeds [25,26]. The Lagrangian implementation uses a triangular mesh that is changed with every step of the simulation. At the initial stage only the boundaries are specified, as the program fills the area with a regular distribution of vertices at a given density. The stresses across this grid are then calculated from the constitutive parameters (such as stress and orientation information) and boundary conditions, and a solution found for the velocities and pressures at each vertex. The triangular elements deform according to these velocities, and the constitutive parameters, which are associated with the elements rather than vertices, updated to reflect the deformations. The grid is checked to split triangular elements that have become too large, delete those which have become too small, and add new elements at inflow boundaries, before moving to the next step. The simulation is by nature time dependent, with each step representing a small movement forward in time, and can be applied only to differential constitutive models due to the prohibitive requirement to track all past history for an integral model. We have used the multi-mode Pom-Pom constitutive model as implemented in flowSolve. A previous application of this method to an MPR flow problem can be found in [23,27].

Table 2
Linear viscoelastic parameters for monodisperse polystyrenes at 200 °C

λ_i (s)	Durham 66k PS (g_i (Pa))	λ_i (s)	Dow PS1569 (g_i (Pa))	Durham 250k PS (g_i (Pa))	Durham 485k PS (g_i (Pa))	Dow PS1571 (g_i (Pa))
0.001	54302	0.01	146610	116150	51748	33232
0.003728	7080.5	0.03728	17198	32265	39229	21098
0.013895	132.65	0.13895	1640.8	15338	29416	29340
0.051795	84.859	0.51795	14.003	1078.7	22430	25839
0.19307	2.0371	1.9307	1.6217	43.087	6383.6	48506
0.71969	1.3697	7.1969	1.3406	4.2688	347.87	8691.9
2.6827	0.4463	26.827	0.18618	0.008243	28.908	2.4291
10	2.7035	100	0.000975	11.079	11.481	48.731

4. Results

4.1. Characterisation

The linear viscoelastic spectra for each of the polystyrenes calculated from small amplitude frequency sweep data by the ARES rotational rheometer are given in Tables 2 and 3. The non-linear Wagner damping factors determined from step strain experiments with the same instrument are given in Table 4. The non-linear parameters for the Pom-Pom model were not able to be determined directly from characterisation experiments, and the values used are discussed in Section 4.5 below.

4.2. Processing of monodisperse polystyrenes

Some features of the flow birefringence fringe patterns were common to all the polystyrenes. The dark areas, shown for example in Fig. 3, at the sides of the slit inserts, represent regions of low stress as they are essentially dead zones with little flow of material. The lighter areas in the main flow stream show dark fringes approaching either the slit entry or exit and illustrate where the stress has reached the level which is the equivalent contour interval between fringes. Monochromatic light was used to generate clear fringes, but these do not reveal the order of the fringes – this could be inferred by viewing the birefringence using white light when a spectrum of colours could be seen with violet at the lower stress side and green at the higher. As well as the increase in stress from the upstream and downstream channels towards the slit entry and exit there was a decrease in stress along the centre line within the slit where the melt is relaxing, while the maximum stress levels could be found at the walls of the slit. As would be expected, for all the materials the overall pressure drop across the slit and the observed number of fringes, increased with increasing flow rate, and decreased with increasing temperature. In all of the following figures, the flow direction through the slit is from top to bottom of the page.

Table 3
Linear viscoelastic parameters for polydisperse polystyrenes at 200 °C

λ_i (s)	80%/20% blend (g_I (Pa))	90%/10% blend (g_i (Pa))	Dow PS680E (g_i (Pa))
0.01	60242	51758	36514
0.03728	18616	16917	19314
0.13895	12794	18721	5256.7
0.51795	6603.0	10072	203.23
1.9307	1089.1	2335.9	4.2001
7.1969	38.148	130.59	1.9137
26.827	0.015912	0.44997	0.56714
100	4.0118	9.1593	0.000191

Table 4
Wagner damping factors for all polystyrenes at 200 °C

	k
Durham 66k PS	0.17
Dow PS1569	0.35
Durham 250k PS	0.22
Durham 485k PS	0.25
Dow PS1571	0.65
80% 485k/20% 66k blend	0.2
90% 485k/10% 66k blend	0.31
Dow PS680E	0.19

It was possible to distinguish between the different materials by examining their birefringence patterns closely. The range of monodisperse polystyrenes showed a clear trend in their fringe patterns as the non-linear character of the flow increased, whether by increasing flow rate or by increasing molecular weight. For low molecular weight monodisperse material at low flow rates (corresponding to low Weissenberg numbers) there was a high degree of symmetry between the entry and exit flow – see Fig. 3(a) for an example. The fringe patterns were essentially symmetric in the upstream and downstream areas and also within the slit and this indicated a “Near Newtonian” behaviour where similar simulations would be predicted using for example Newtonian or power law simulation. As the flow rate increased this symmetry was gradually eroded, with the nested continuous isochromatics within the slit moving downstream, and the number of fringes in the downstream channel dropping below the number of their upstream counterparts. Fig. 3(b) shows an example of an “asymmetric” monodisperse fringe pattern at intermediate flow conditions. We have defined this regime of flow “viscoelastic asymmetric”. For the two highest molecular weight samples studied, and hence at still higher Weissenberg numbers, we observed a transition to an unstable flow regime which is reported in detail in the following section.

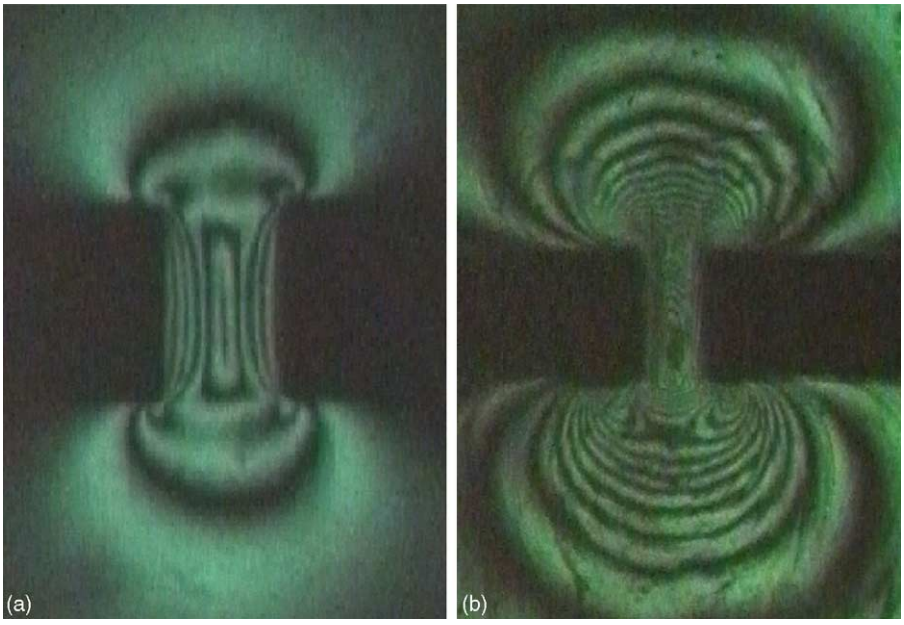

Fig. 3. Example flow birefringence of monodisperse polystyrenes at 200 °C; (a) slow flow (We ≈ 1): PS1569, piston speed 0.2 mm/s; (b) intermediate flow (We ≈ 50): PS1571, piston speed 0.1 mm/s.

4.3. Processing instabilities

Study of the monodisperse Dow PS1571, with a molecular weight of 510,000 kg/kmol, revealed an unstable break-up of flow at higher flow rates with two distinctive types of instability. At low flow rates, the fringe patterns conformed to the asymmetric layout of a typical medium molecular weight monodisperse, but instead of a steady pattern there was a regular continuous oscillation. The number of fringes was observed to increase suddenly, then relax more gently before the next sudden increase. The frequency of this pulsing instability was observed to be proportional to flow rate, as illustrated in Fig. 4. Whilst the pulsing cannot be seen at higher flow rates, another more dramatic type of instability was observed, which we have termed *viscoelastic disturbance*.

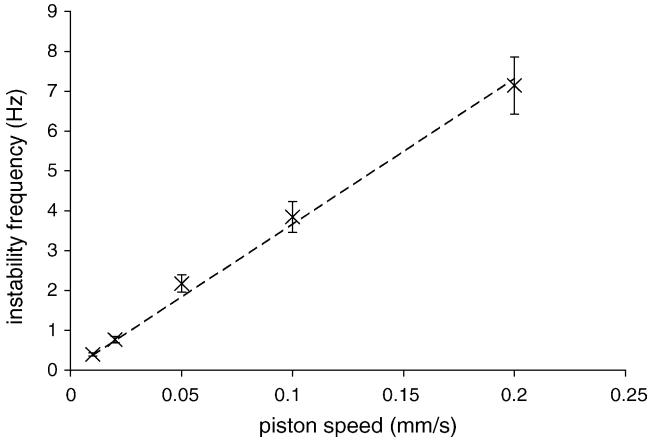

Fig. 4. Change in frequency of pulsing instability; Dow PS1571 at 180 °C.

The birefringence pattern within and downstream region of the slit was seen to break up completely, with a random fluctuations of dark and light instead of clear continuous fringes. Upstream of the slit the fringes were continuous, but distorted and also unsteady as there was a distinct side-to-side oscillation. Although these dynamic effects are difficult to depict on the printed page, Fig. 5 shows example still images from the two types of instability.

Though the effect of the instabilities on the birefringence is most dramatic downstream of the slit, more upstream detail can be seen by removing the polarisers and studying the resultant bright field images, as shown in Fig. 6. Dark areas were seen around the slit where the light has been distorted from its straight line path, either as a result of refraction caused by localised shear heating or in areas where the melt was no longer homogeneous. Substantial dark areas along the slit wall were seen, as well as fluctuating dark regions upstream converging on the slit entry corners. Downstream of the slit there were persistent dark lines, curved in an arc approximately centred on the slit exit and being alternately shed from either side of the slit. We interpret some of the dark regions as areas where there is a high refractive index gradient within the melt that was caused by a "non continuum flow" where smooth variations in stress, velocity and or density do not exist.

4.4. Processing of polydisperse polystyrenes

The Flow birefringence of both broad molecular weight polydisperse or bimodal monodisperse blends shown in Fig. 7 could be differentiated from their monodisperse counterparts. A strong asymmetry between the slit entry and exit, was present at all piston speeds tested, and instabilities were not

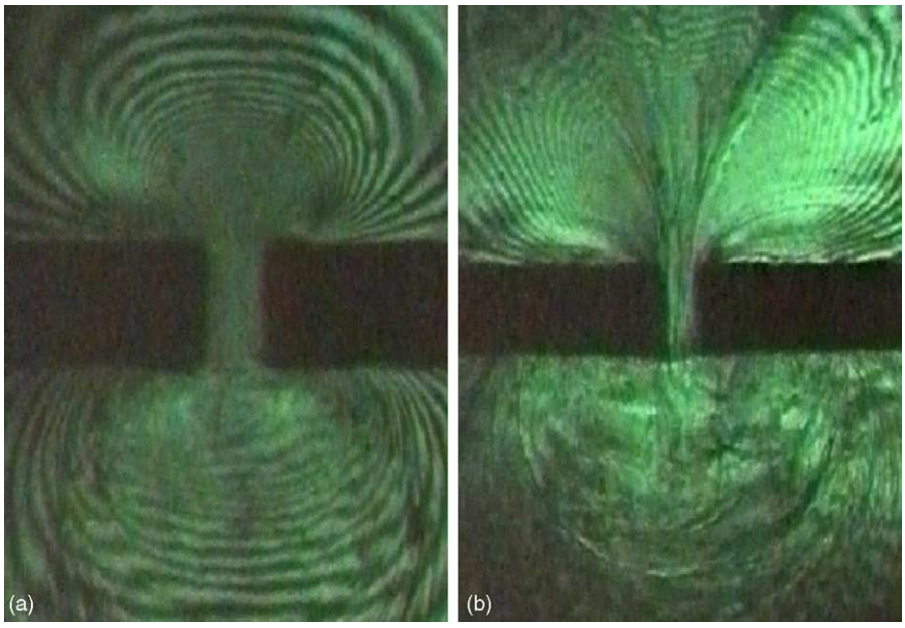

Fig. 5. Flow birefringence of PS1571 at 200 °C; (a) pulsing instability, piston speed 0.5 mm/s; (b) viscoelastic disturbance, piston speed 2 mm/s.

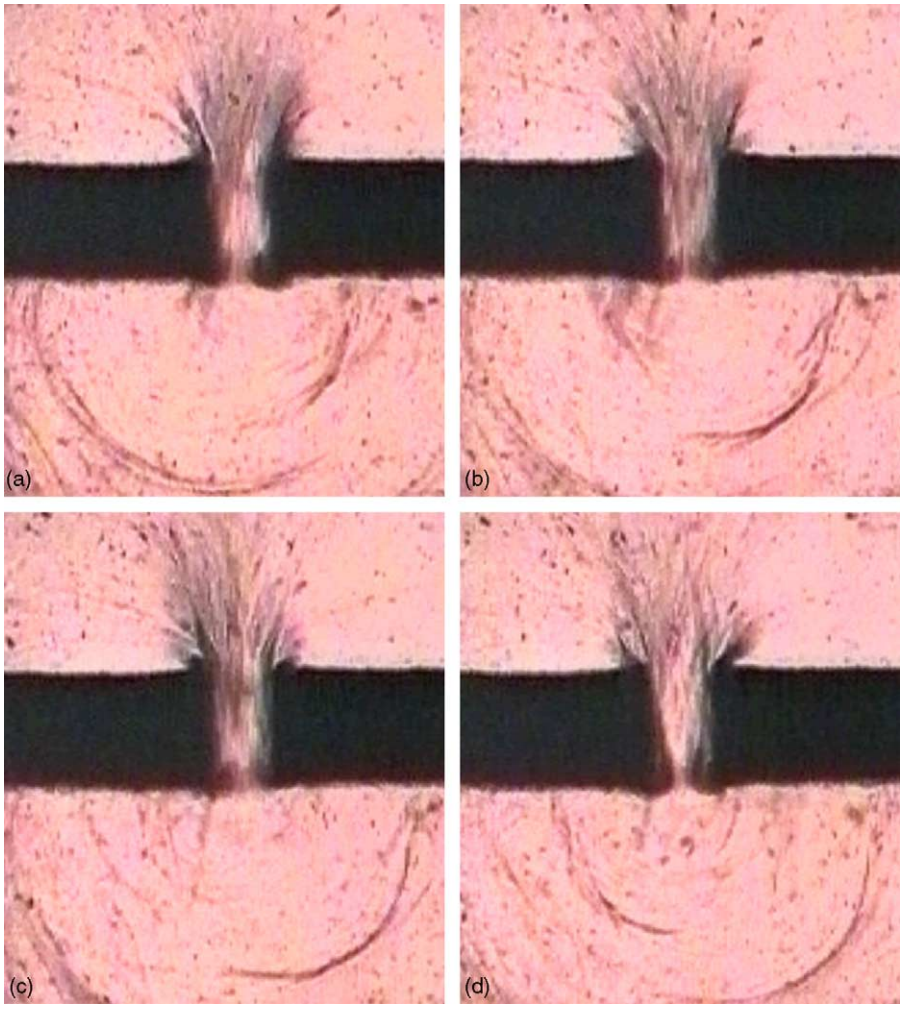

Fig. 6. Bright field observations of Dow PS1571 PS at 180 °C; piston speed 1.0 mm/s; time interval between frames (a)–(d) 0.2 s.

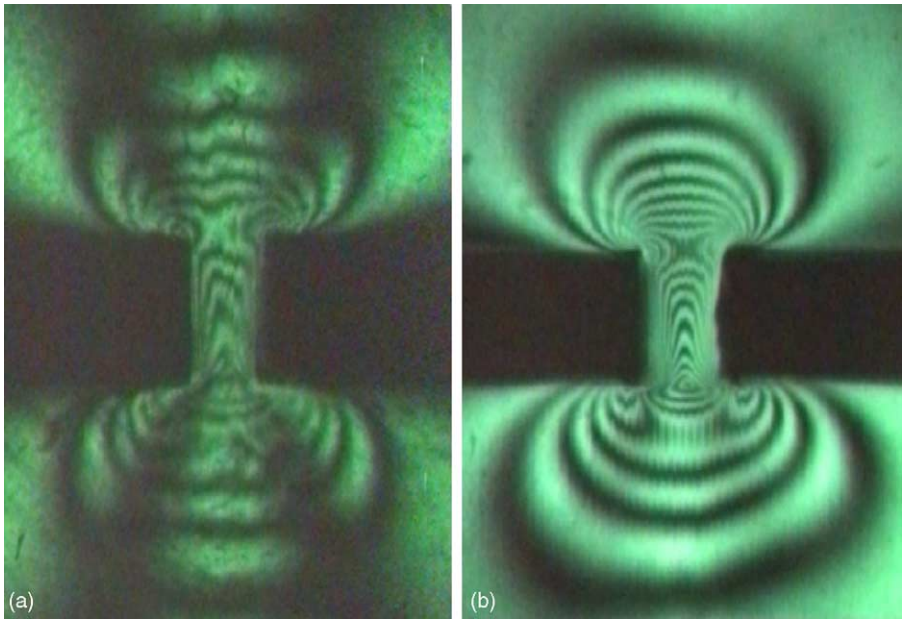

Fig. 7. Example flow birefringence of bimodal blend and broadly polydisperse polystyrenes at 200 °C; (a) 90%/10% 485k/66k PS blend, piston speed 0.2 mm/s; (b) PS680E, piston speed 2 mm/s.

observed for the range of piston speeds used. The monodisperse Durham 485k PS had exhibited instabilities at high flow rates, but when this material was blended with a small proportion of a low molecular weight component (Durham 66k PS), the resulting polymer was much easier to process than the 485k alone and no instabilities were observed. Doubling the proportion of the low molecular weight component from 10 to 20% led to further improvement in processability, but not as dramatic as the impact of the addition of the initial 10% – to quantify this, for a given piston speed of 0.5 mm/s the pressure difference across the slit at 200 °C was 10.3 bar for the 485k alone, reduced to 4.4 bar for the 10% blend and 3.7 bar for the 20% blend. Similarly, the broadly polydisperse Dow PS680E was significantly easier to pro-

Table 5
Summary of flow regimes observed experimentally at 200 °C

designation	type	piston speed (mm/s) 0.1 1 10
Durham 66k	Monodisperse low MW	NN
Dow 1569		NN, VA
Durham 250k		NN, VA
Durham 485k		VA, UF
Dow 1571	high MW	VA, UF
Durham 80/20%	blend	VA
Durham 90/10%		VA
Dow 680E	polydisperse	VA

NN = near Newtonian, VA = viscoelastic asymmetric, UF = unstable flow.

cess than monodisperse polystyrene of a similar molecular weight. Fig. 7 shows examples of the observed birefringence pattern for both types of polydisperse material. The presence of polydispersity, whether from a commercial polymerization or from blending monodisperse polymers broadens the processing window of the material where stable viscoelastic flow can occur.

Table 5 below gives a visual summary of the flow regimes seen for each of the polystyrene samples under test at 200 °C. The flow types described in the last three sections have been divided into "Near Newtonian", "Viscoelastic Asymmetric" and "Unstable Flow" conditions.

4.5. Numerical simulation

The application of both Polyflow and flowSolve to numerical prediction of our results provides an opportunity to compare the two numerical and constitutive approaches with each other as well as the experimental birefringence. The main comparative factors used were the magnitude of the overall pressure difference across the slit (to which the magnitude of the stress is closely related) and the shape of the principal stress difference contour pattern. The latter can be related to the observed birefringence using the stress–optical relation [28] given as Eq. (3). This links the refractive index and stress

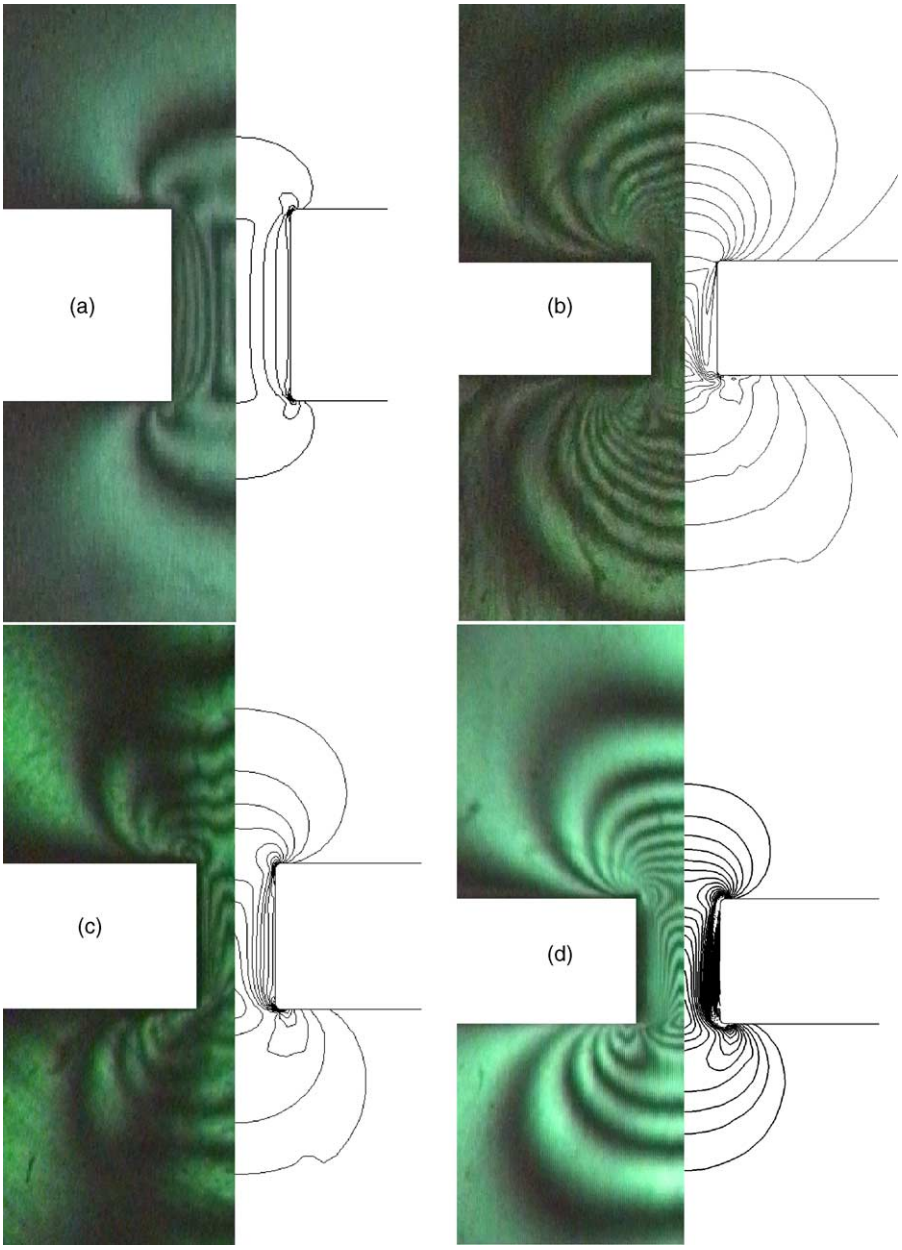

Fig. 8. Comparison of experimental birefringence with principal stress difference contour prediction made by Polyflow using the Wagner model for polystyrenes at 200 °C; (a) monodisperse Dow PS1569, piston speed 0.2 mm/s; (b) monodisperse Dow PS1571, piston speed 0.1 mm/s; (c) Durham 90%/10% 485k/66k PS blend, piston speed 0.2 mm/s; (d) polydisperse Dow PS680E, piston speed 2 mm/s.

tensors by the constant of proportionality C, the stress–optical coefficient, which depends on the chemical structure of a material. The stress–optical coefficient has been found to be independent of molecular (as opposed to chemical) structure, and almost independent of temperature above 150 °C for polystyrene, and to have the value -4.5×10^{-9} Pa^{-1} [29]. This equates to an appropriate principal stress difference contour interval for equivalence to the isochromatic extinction bands of 11.4 kPa, which has been used for all the contour plots shown. Two-dimensional, isothermal flow was assumed for both simulations, and steady state conditions in the case of Polyflow.

$$\boldsymbol{n} = C\boldsymbol{\sigma} \tag{3}$$

Side-by-side comparisons between experimental birefringence patterns and principal stress difference contours predicted by Polyflow using the Wagner model are given in Fig. 8 for examples of both monodisperse and polydisperse polystyrenes. Most of the constitutive parameters for the Wagner model have been given in Section 4.1 above, the exception being β. This has been found experimentally to be close to 0.02 for three different polymers, and 0.022 in the case of polystyrene [30], although it is not actually significant in two-dimensional numerical simulations. In addition to the constitutive equation, in Polyflow there are three areas of the numerical method itself that must be specified: the shape, size and distribution of the quadrilateral elements in the mesh; the iteration and numerical integration methods used; and the convergence criterion that determines when a result has been reached. A mesh based on examples for similar entry and exit flows was used, with elements concentrated in the corner regions. Adjustment of the numerical methods from their defaults was necessary to achieve convergence, but the convergence criterion is the key parameter to determine the accuracy of the result – for most of the flow conditions simulated this was set at 10^{-3} for the final convergence stage.

For most of the materials, the shapes of the predicted and observed fringe patterns were a reasonable match. They reflected high symmetry for low molecular weight monodisperse samples at all flowrates and for higher molecular weight monodisperse at high flowrates. Equally asymmetry was seen for the blends and polydisperse sample. In all these cases the direct matching of contours to fringes was best within the slit, and weaker further away in the main channel. The poor fit away from the channel may be a consequence of the two-dimensional assumption for both fringes and simulation. For the high molecular weight monodisperse material where flow instabilities were seen experimentally, Polyflow was unable to converge to a solution. The predicted pressure differences across the slit were close to the measured values for all the materials at low flow rates, but at higher flow rates there was a trend for the numerical solution to overpredict the pressure difference for low molecular weights and underpredict the pressure difference for high molecular weights. Fig. 9 shows

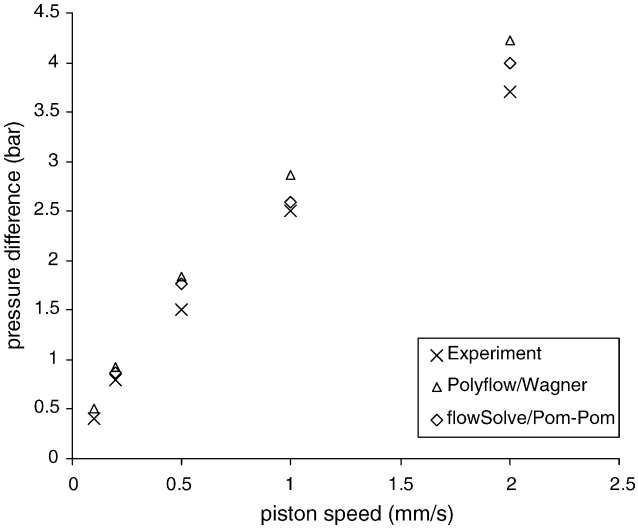

Fig. 9. Comparison of experimental pressure difference with predicted values for PS680E at 200 °C.

a sample comparison between measured and predicted pressure differences.

While the single experimentally determined exponential non-linear parameter for the Wagner model could be measured experimentally, this was impractical for the many more adjustable non-linear parameters in the Pom-Pom model (three per mode, 18 in total in this case). The backbone orientation relaxation times τ_{bi} and moduli g_i are the linear relaxation spectrum, leaving the backbone stretch relaxation times τ_{si}, numbers of arms q_i and drag-strain coupling parameters n_i^* to vary for each mode. The last of these is simple to deal with as [20] recommends that this be fixed equal to $2/q_i$. A crude method of fitting the other two parameters to experimental data for polyethylene is described in [19] but this could not be used in this case as the required transient uniaxial extension data was not available.

To be consistent with the physical model, the ratio between the backbone orientation and stretch relaxation times was constrained to the approximate range 2–10, and τ_{si} must be less than $\tau_{b(i-1)}$ [19] which restricts this still further. In previously published sets of Pom-Pom parameters the ratio generally decreases with increasing relaxation time. Finally, as q_i is a measure of the order of branching and we know that the polystyrenes studied are linear molecules we would expect it to be low, and $q_i = 1$ was suggested. To test the plausibility of these parameters, experimental transient shear viscosity was measured and compared to Pom-Pom predictions for this flow – it was seen that variations of the timescale ratio within its limited range made no discernable difference to the shear prediction, while increasing q_i worsened the prediction.

The details of the flowSolve calculations are less directly controlled than in Polyflow, but one of the variables proved to be significant. The triangular Lagrangian mesh evolves in time with the problem, with the user-specified information being the boundaries, initial point density, and length and area

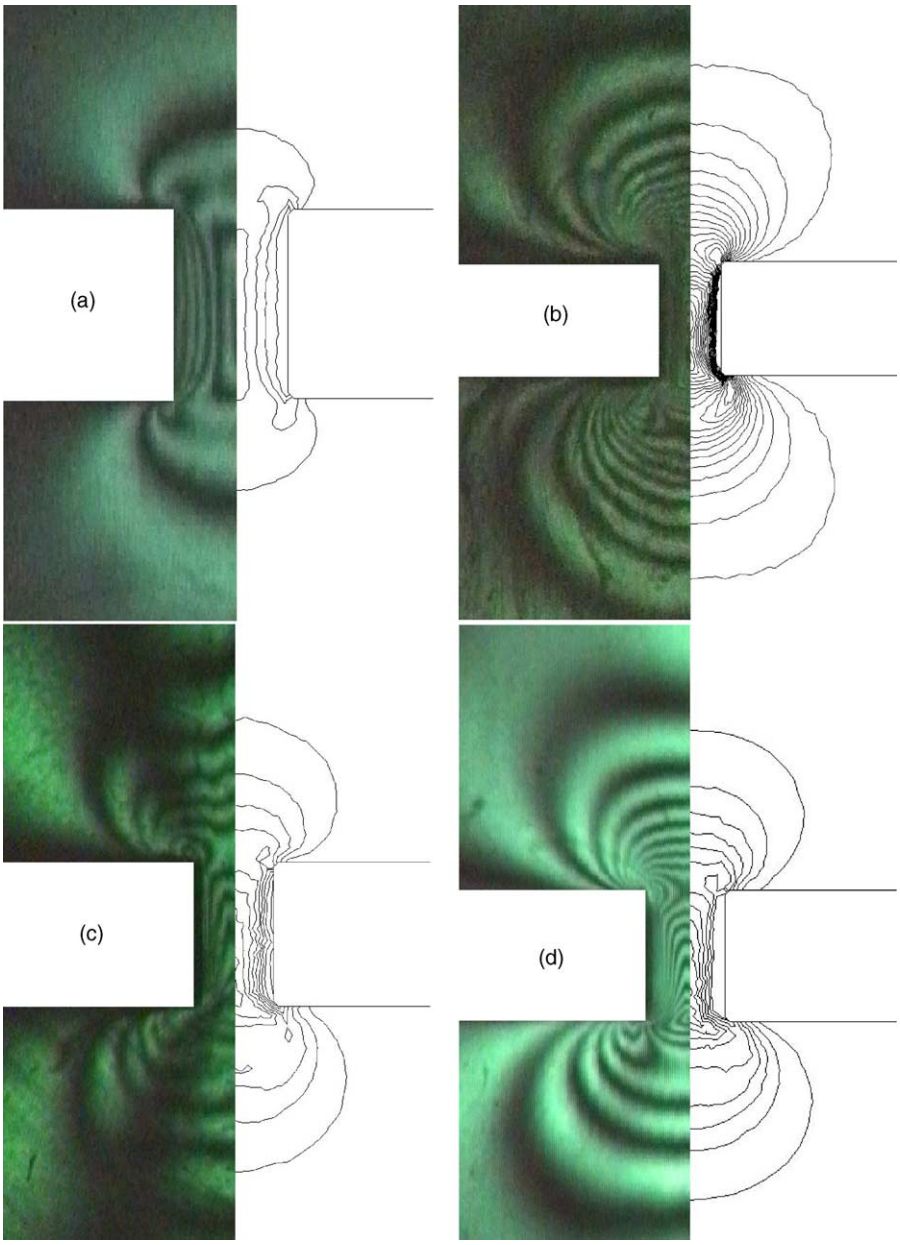

Fig. 10. Comparison of experimental birefringence with principal stress difference contour prediction made by flowSolve using the Pom-Pom model for polystyrenes at 200 °C; (a) monodisperse Dow PS1569, piston speed 0.2 mm/s; (b) monodisperse Dow PS1571, piston speed 0.1 mm/s; (c) Durham 90%/10% 485k/66k PS blend, piston speed 0.2 mm/s; (d) polydisperse Dow PS680E, piston speed 2 mm/s.

restrictions for re-meshing. Convergence problems encountered were avoided by reducing the mesh and time step size, and when this did not occur the result reached was independent of these variables. The most important parameter of all was found to result from the way in which the calculations were made – not all of the relaxation modes were calculated explicitly using the Pom-Pom equations, but the faster modes were considered to be purely viscous. Any number of modes can be considered "fast" as long as there is at least one fast and one slow, and this number had a significant impact on the final result (stresses were approximately twice as high with seven fast modes as with one). The results we have considered to be the Pom-Pom model predictions are those with just one fast mode, that is with all other modes calculated in full.

Comparisons between experimental birefringence and predicted stress for flowSolve using the Pom-Pom model are given in Fig. 10 for the same materials and flow conditions as shown earlier. The overall effect is similar to Polyflow: the shapes of the predicted and observed fringe patterns were a good match for most of the materials. Symmetry and asymmetry between the slit entry and exit flow was predicted as expected, with trends for increasing asymmetry as molecular weight, flow rate and polydispersity increase. In contrast to Polyflow, flowSolve was able to predict stresses for high

molecular weight monodisperse polystyrene at the flow rates where instabilities were observed, but did not predict the instabilities themselves.

5. Discussion and conclusions

A key experimental observation reported in this paper is that the stable processing of monodisperse polystyrene occurred in a "Near Newtonian" way giving symmetric entry/exit fringe patterns. For some of the monodisperse polymers there was a small flow region where, if the molecular weight was high enough the fringe pattern becomes asymmetric, but a further increase in flow rate or molecular weight resulted in the flow pattern becoming irregular and the flow unstable. By contrast, both the monodisperse blend and polydisperse material showed stable asymmetric viscoelastic fringes over a wide range of flow rates. This result indicates that for these polymers the asymmetry is the result of the wider range of timescales present in the relaxation spectrum and for most processing conditions, some timescales are long in relation to the experimental transit time through the slit.

A further result of the experimental work is the demonstration of the breakdown of continuum flow for the processing of high molecular weight monodisperse polystyrenes which starts with a pulsing instability and increases to a viscoelastic disturbance. These effects were visible using both birefringence and bright field optical methods but could not be inferred from pressure difference alone. Localised shear heating appears to have occurred at the slit walls and in fluctuating regions upstream from the entry corners. The dark lines upstream of the entrance, and persistent curved lines downstream of the exit, may be caused by the melt separating into layers in a region of high stress, with the boundaries between these being a region with fewer entanglements that allows the adjoining layers to flow more easily past each other.

The bimodal blends, containing a small proportion of a low molecular weight component, required a significantly lower pressure to process than the bulk high molecular weight component alone, while the doubling of this proportion made a further improvement to processability but a diminishing return. The commercial broadly polydisperse material was again significantly easier to process than a monodisperse polystyrene of similar molecular weight. These results illustrate the important role played by low molecular weight components in improving processability, as the shorter chains are able to realign and relax much more quickly than longer molecules in the high stress regions of a flow geometry. However, useful narrowly monodisperse materials may be as an aid to understanding processing flows, polydispersity is desirable for commercial applications where ease of processing is important.

For any study that uses two-dimensional numerical simulations to model real systems, the extent to which they can be assumed to be equivalent must be considered. The design of the MPR slit flowcell, with the width of the slit being an order of magnitude smaller than the depth of the optical path through it, was intended to minimise the impact of wall effects so that the fringe patterns observed in the melt were approximately equivalent to a two-dimensional slice taken from the main body of the flow channel. It has been predicted that in channels with this aspect ratio boundary layers near the walls will affect apparent retardation by only a few percent [31], while previous experimental studies comparing birefringence to simulation (for example [7]) have shown that this appears to be a valid assumption. Away from the slit area, however, the channel has a square cross-section and wall effects are likely to be more significant – this is likely to be the reason that the match between experiment and simulation was seen to be better within the slit.

We have used two different combinations of numerical solver and constitutive model to simulate processing flows of monodisperse and polydisperse polystyrenes, in order to test their predictions with experiment. In practice, both were able to make reasonable predictions for both the pressure difference across the slit and the stress distribution within the slit. Polyflow and the Wagner model had convergence problems with all of the materials at higher flow rates, in particular with the high molecular weight monodisperse where experimental instabilities were seen. Since these instabilities reflect the material's inability to deform in a well-behaved, predictable manner when subject to the imposed flow conditions, it may be that the constitutive equation was unable to describe them rather than the problems arising from numerical approximations. In contrast to this, flowSolve using the Pom-Pom model was able to make predictions at much higher flow rates, though these did not predict instability. This is likely to be due to the method used in the solver, which requires there to be at least one fast relaxation mode that is treated as Newtonian. Because each numerical solver used different constitutive equations and different methods for numerical solution it was not possible from the results described here to explicitly rank constitutive equation or numerical code performance independently.

From the experimental work described in this paper it is possible to establish trends in the similarities and differences between the processibilty of monodisperse and polydisperse polymers. The matching of numerical simulation data to experimental results indicates that the empirically based Wagner integral constitutive equation and the molecularly based Pom-Pom constitutive equation both capture elements of the steady flow processing behaviour. However, neither predict the transition of flow at and beyond the experimentally observed stable regime.

Acknowledgements

We would like to acknowledge the funding of this work by EPSRC, through the Microscale Polymer Processing Project; the supply of polystyrene samples by Dow Chemicals and the University of Durham; and the University of Leeds for

the use of flowSolve. Prof. T. McLeish is to be thanked for masterminding the Microscale project.

References

[1] R. Ahmed, R.F. Liang, M.R. Mackley, The experimental observation and numerical prediction of planar entry flow and die swell for molten polyethylene, J. Non-Newtonian Fluid Mech. 59 (1995) 129.
[2] F.P.T. Baaijens, S.H.A. Selen, H.P.W. Baaijens, G.W.M. Peters, H.E.H. Meijer, Viscoelastic flow past a confined cylinder of a low density polyethylene melt, J. Non-Newtonian Fluid Mech. 68 (1997) 173.
[3] K. Lee, M.R. Mackley, The significance of slip in matching polyethylene processing data with numerical simulation, J. Non-Newtonian Fluid Mech. 94 (2000) 159.
[4] D.V. Boger, M.J. Crochet, R.A. Keiller, On viscoelastic flows through abrupt contractions, J. Non-Newtonian Fluid Mech. 44 (1992) 267.
[5] M.R. Mackley, R.T.J. Marshall, J.B.A.F. Smeulders, The multipass rheometer, J. Rheol. 39 (1995) 1293.
[6] M.R. Mackley, P.H.J. Spitteler, Experimental observations on the pressure-dependent polymer melt rheology of linear low density polyethylene using a multi-pass rheometer, Rheol. Acta 35 (1996) 202.
[7] K. Lee, M.R. Mackley, The application of the multi-pass rheometer for precise rheo-optic characterisation of polyethylene melts, Chem. Eng. Sci. 56 (2001) 5653.
[8] F.P.T. Baaijens, Mixed finite element methods for viscoelastic flow analysis: a review, J. Non-Newtonian Fluid Mech. 79 (1998) 361.
[9] T.C.B. McLeish, R.C. Larson, Molecular constitutive equations for a class of branched polymers: the Pom-Pom polymer, J. Rheol. 42 (1998) 82.
[10] B. Bernstein, E.A. Kearsley, L.J. Zapas, A theory of stress relaxation with finite strain, Trans. Soc. Rheol. 7 (1963) 391.
[11] V.M. Kamath, M.R. Mackley, Determination of polymer relaxation moduli and memory functions using integral transforms, J. Non-Newtonian Fluid Mech. 32 (1989) 119.
[12] M.R. Mackley, R.T.J. Marshall, J.B.A.F. Smeulders, F.D. Zhao, The rheological characterization of polymeric and colloidal fluids, Chem. Eng. Sci. 49 (1994) 2551.
[13] G.G. Fuller, Optical rheometry of complex fluids, Oxford University Press, 1995.
[14] J.D. Ferry, Viscoelastic Properties of Polymers, Wiley, New York, 1980.
[15] R.G. Larson, Constitutive Equations for Polymer Melts and Solutions, Butterworths, Boston, 1988.
[16] M. Doi, S.F. Edwards, The Theory of Polymer Dynamics, Oxford University Press, 1986.
[17] M.H. Wagner, Analysis of time dependent stress growth data for shear and elongational flow of a low density polyethylene, Rheol. Acta 18 (1979) 33.
[18] M.H. Wagner, S.E. Stephenson, The irreversibility assumption of network disentanglement in flowing polymer melts and its effects on elastic recoil predictions, J. Rheol. 23 (1979) 489.
[19] N.J. Inkson, T.C.B. McLeish, O.G. Harlen, D.G. Groves, Predicting low density polyethylene melt rheology in elongational and shear flows with “Pom-Pom” constitutive equations, J. Rheol. 43 (1999) 873.
[20] R.J. Blackwell, O.G. Harlen, T.C.B. McLeish, Molecular drag-strain coupling in branched polymer melts, J. Rheol. 44 (2000) 121.
[21] N. Clemur, R.P.G. Rutgers, B. Debbaut, Numerical simulation of abrupt contraction flows using a double convected Pom-Pom model, J. Non-Newtonian Fluid Mech. 117 (2004) 193–209.
[22] N. Clemur, R.P.G. Rutgers, B. Debbaut, Numerical evaluation of three dimensional effects in planar flow birefringence, J. Non-Newtonian Fluid Mech. 123 (2004) 105–120.
[23] K. Lee, M.R. Mackley, T.C.B. Mcleish, T.M. Nicholson, O. Harlen, Experimental observation and numerical simulation of transient stress fangs within flowing molten polyethylene, J. Rheol. 45 (6) (2001) 1261–1277.
[24] M.J. Crochet, B. Debbaut, R. Keunings, J.M. Marchal, in: K.T. O’Brien (Ed.), Computer Modelling for Extrusion and Other Continuous Polymer Processes, Karl Hanser Verlag, Munich, 1992 (Chapter 2).
[25] O.G. Harlen, J.M. Rallison, P. Szabo, A split Lagrangian-Eulerian method for simulating transient viscoelastic flows, J. Non-Newtonian Fluid Mech. 60 (1995) 81.
[26] T.M. Nicholson, FlowSolve: A Lagrangian Flow Solver for Complex Flows in Polymers – Developers Manual, University of Leeds, 2000.
[27] G.B. Bishko, O.G. Harlen, T.C.B. McLeish, T.M. Nicholson, Numerical simulation of the transient flow of branched polymer melts through a planar contraction using the Pom-Pom model, J. Non-Newtonian Fluid Mech. 82 (1999) 255.
[28] A.S. Lodge, Variation of flow birefringence with stress, Nature 176 (1955) 838.
[29] H. Janeschitz-Kriegl, Polymer Melt Rheology and Flow Birefringence, Springer-Verlag, New York, 1983.
[30] A.C. Papanastasiou, L.E. Scriven, C.W. Macosko, An integral constitutive equation for mixed flows: viscoelastic characterisation, J. Rheol. 27 (1983) 387.
[31] S.R. Galante, P.L. Frattini, The influence of end effects on birefringence measurements in nominally two-dimensional channel flows, J. Rheol. 35 (1991) 1551.